

Inferring clonal composition from multiple tumor biopsies

Matteo Manica^{1,2,*}, Philippe Chouvarine^{3,*}, Roland Mathis^{1,*}, Ulrich Wagner⁴, Kathrin Oehl⁴, Karim Saba⁴, Laura De Vargas Roditi⁴, Arati N Pati³, María Rodríguez Martínez¹, Peter J. Wild⁴, Pavel Sumazin³

¹ IBM Research—Zurich, 8803 Rüschlikon, Switzerland

² Institute of Molecular Systems Biology, ETH Zurich, Zurich, Switzerland

³ Texas Children's Cancer Center, Baylor College of Medicine, Houston, Texas, USA

⁴ Pathology and Molecular Pathology, University Hospital Zurich, Zurich, Switzerland

* Joint first authors Correspondence to sumazin@bcm.edu

Abstract

Motivation. Knowledge about the clonal evolution of each tumor can inform driver-alteration discovery by pointing out initiating genetic events as well as events that contribute to the selective advantage of proliferative, and potentially drug-resistant tumor subclones. A necessary building block to the reconstruction of clonal evolution from tumor profiles is the estimation of the cellular composition of each tumor subclone (*cellularity*), and these, in turn, are based on estimates of the relative abundance (*frequency*) of subclone-specific genetic alterations in tumor biopsies. Estimating the frequency of genetic alterations is complicated by the high genomic instability that characterizes many tumor types.

Results. Analysis of our mutation-centric model for genomic instability suggests that copy number variations (CNVs) that are commonly observed in tumor profiles can dramatically alter mutation-frequency estimates and, consequently, the reconstruction of tumor phylogenies. We argue that detailed accounting for CNVs based on profiles of multiple biopsies for each tumor are required to accurately estimate mutation frequencies. To help resolve this problem we propose an optimization algorithm—Chimæra: clonality inference from mutations across biopsies—that accounts for the effects of CNVs in multiple same-tumor biopsies to estimate both mutation frequencies and copy numbers of mutated alleles. We show that mutation-frequency estimates by Chimæra are consistently more accurate in unstable genomes. When studying profiles of multiple biopsies of a high-risk prostate tumor, we show that Chimæra inferences allow for reconstructing its clonal evolution.

Data availability. Sequencing data is deposited in ENA project PRJEB19193 and source code in GitHub project Chimaera.

Introduction

Pan-cancer tumor profiling has identified recurrent alterations that are associated with tumor etiology at the loci of thousands of genes (Futreal, et al., 2004; Higgins, et al., 2007). Yet, despite this wealth of information, patient genomic profiles often fail to reveal tumorigenesis-driving alterations, and, consequently, the interpretation of genomic alterations remains a major challenge for personalized medicine efforts in oncology. Knowledge about tumor clonal evolution can point to genomic alterations that both contribute to tumorigenesis and indicate prognostically-relevant intratumoral variability (Fidler and Hart, 1982; Nowell, 1976). Specifically, clonal evolution—depicted as a phylogenetic tree in Figure 1A—can help identify alterations that play a role in tumor initiation as well as those that confer a selective advantage to altered tumor cells. In addition, information about the subclonal composition of tumors is essential for designing targeted therapies, since not all subclones may be targeted in the same way. Indeed,

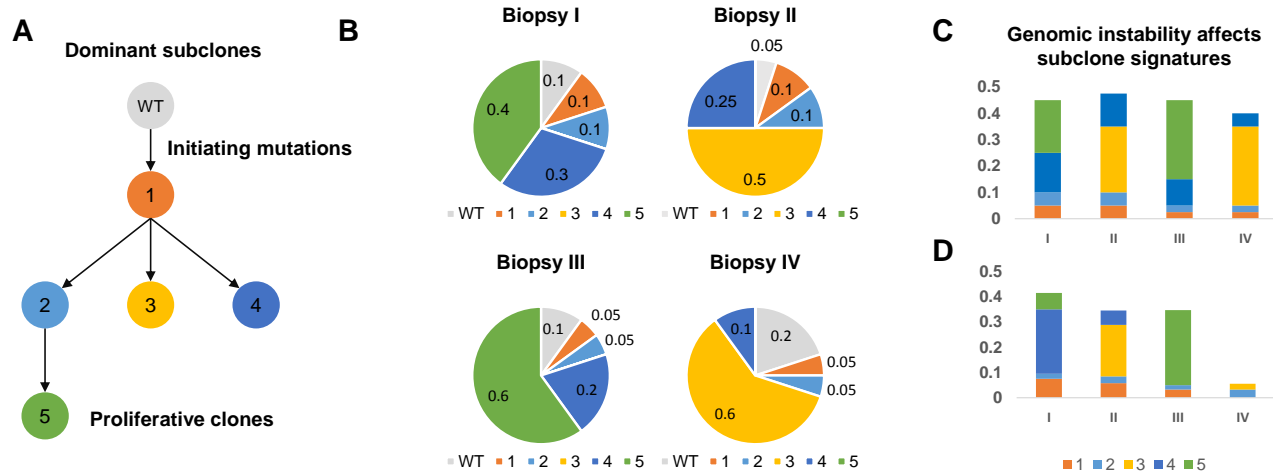


Figure 1. Footprint of clonal evolution across tumor biopsies. **(A)** Tumor phylogeny composed of five dominant tumor subclones and wildtype (WT) cells—with no somatic mutations—that make up the cellular composition of four tumor biopsies **(B)**. Subclones 3 and 5 were more proliferative—i.e. the proportion of these subclones (*cellularity*) in containing biopsies is greatest. **(C)** Failure to account for genomic instability can skew cellularity estimates because fractions of reads (*mutated-read fractions*) presenting each mutation in WES depend on the copy numbers of the alleles in both mutated and non-mutated cells. Consequently, in genomically-stable tumors, biopsies from **(B)** will have mutated-read fractions that differ from those of **(D)** genomically unstable tumors with the same cellularities.

tumor heterogeneity may hold the key to predicting tumor progression, sensitivity to a drug, and prognosis, as drug resistance and metastatic potential may vary between subclones (Boutros, et al., 2015).

Current methods that rely on DNA-profiling to reconstruct tumor clonal evolution can be classified into two categories: methods that primarily rely on single-cell sequencing (Gao, et al., 2016; Mann, et al., 2016; Suzuki, et al., 2015; Wang, et al., 2014) and those that computationally resolve mixtures of subclones from molecular profiles of tumors, i.e. profiles of pools of cells originating from a common malignant lesion (Andor, et al., 2016; El-Kebir, et al., 2015; Niknafs, et al., 2015). Single-cell sequencing can produce more definitive estimates of the proportion of tumor cells that contain each genomic alteration (alteration frequency) and more complete profiles of tumor subclones including information about the co-occurrence of alterations in each subclone. The primary disadvantages of single-cell methods are operational—the availability of high-quality snap-frozen or fresh tumor samples that permit single-cell isolation, and the accuracy and cost associated with sequencing DNA from hundreds of single cells per tumor. Costs associated with single-cell library preparation may not decline as rapidly as the cost of sequencing, and accuracy is likely to remain an issue due to limited material availability in single cells. Moreover, the availability of tissue for single-cell isolation is not likely to improve as future sequencing technologies focus on profiling formalin-fixed paraffin-embedded (FFPE) tissues that are not fully compatible with single-cell isolation (Cieslik, et al., 2015; Getz and Ardlie, 2012).

We are interested in improving methods for reconstructing clonal evolution from mutation profiles of primary tumors. In the absence of single-cell sequencing, we need to deconvolve mutation frequencies, alteration-subclone associations, and subclone cellularities from sequencing assays that average profiles across cellular ensembles (Figure 1B). One approach to improving the accuracy of this deconvolution is to profile multiple biopsies from the same tumor across time points (Wang, et al., 2014) or across tumor regions that may be selected for their variable

histological presentation (Boutros, et al., 2015; Gundem, et al., 2015). While this approach may not be feasible for all tumor types, due to concerns about clinically unjustified strain to patients, it is a natural fit for high-risk patients with blood malignancies and some solid tumors, including prostate adenocarcinomas. The presence of multiple biopsies can benefit efforts to deconvolve cellularity and tumor phylogeny because, and especially if carefully collected, the clonal composition across regions of heterogeneous tumors is expected to be variable. Consequently, under the infinite-sites assumption (Jiao, et al., 2014) where two genomic events may not target the same locus, genomic alterations that are specific to one tumor subclone will co-occur with the same frequency across biopsies.

Focusing on single-nucleotide somatic variants (SNVs; or simply mutations), we describe the clonality problem as that of associating mutations with subclones and inferring ancestral relations between subclones. The goal of the resulting set-theoretic formulation, for each tumor, is to aggregate co-occurring mutations across biopsies, estimate the frequency of each aggregate in every biopsy, and identify partial orders across aggregates that are consistent across biopsies. When viewed this way, each subclone can be associated with a frequency vector that describes the proportion of cells containing its mutations in each biopsy. Establishing ancestral order between two subclones then depends on comparisons between their corresponding mutation frequencies. Note that subclone cellularity is a function of tumor phylogeny and mutation frequency: daughter subclones inherit mutations from ancestral subclones. Consequently, the cellularity and frequency of a subclone and one of its associated mutations can be 0 and 100%, respectively, if this mutation originated in an extinct ancestral subclone whose descendant subclones populated the profiled tumor.

Our first challenge is to estimate mutation frequencies across biopsies. In cellular environments with stable genomes, where CNVs are few, accurate mutation-frequency estimation is a function of allele coverage. Mutation frequencies can be computed directly from sequencing evidence for the mutated allele—the fraction of reads (*mutated-read fraction*) that support the mutation as observed in whole-exome sequencing (WES) data. However, CNVs can affect mutation frequency estimates because the mutated-read fraction is affected by contributions from alleles in mutation-free cells as well as both the mutated and wildtype forms of the allele in mutated cells. Changes to the copy number of one of these allele contributors can alter the mutated-read fraction dramatically, and if not accounted for, will result in inaccurate mutation-frequency estimates (Figure 1C). In turn, errors in mutation-frequency estimates can translate to inaccurate phylogeny reconstruction (Figure 2).

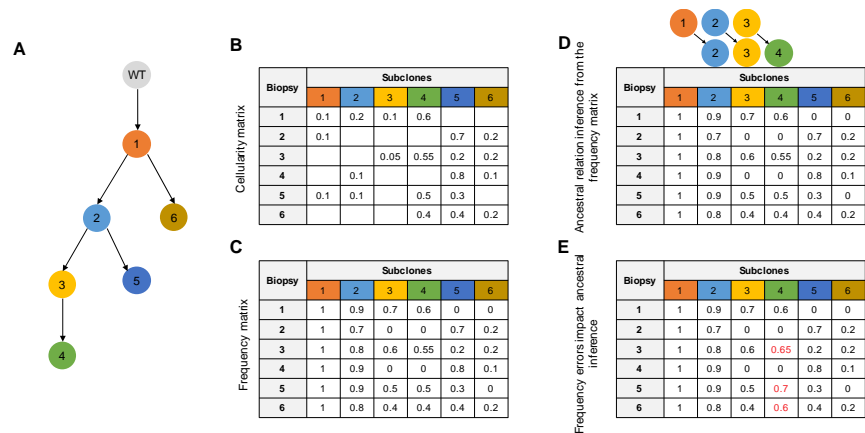


Figure 2. Small variations in mutation frequency estimates can impact the inference of ancestral relations. (A) Simulated tumor phylogeny, (B) subclone cellularities, and (C) frequencies of subclonal mutations across biopsies. (D) Ancestral relations between subclones can be inferred from comparisons of their frequency vectors: Subclone 4 frequencies are greater than those of subclone 3 across all biopsies, but (E) errors in frequency estimates (red) can violate this relationship and complicate tumor-phylogeny reconstruction efforts.

Here, we introduce a natural model for the effects of CNVs on mutated-read fractions in WES. We use this model as a basis for simulations with CNV distributions that are compatible with observations from The Cancer Genome Atlas (TCGA)-profiled primary breast and prostate adenocarcinomas (The Cancer Genome Atlas, 2012; The Cancer Genome Atlas, 2015). Data was simulated using synthetically generated phylogeny, including CITUP phylogenies (Malikic, et al., 2015), followed by the duplication or loss of sequencing reads according to simulated effects of CNVs. Attempts to estimate the frequencies and cellularities of mutations and subclones using ABSOLUTE (Carter, et al., 2012), AncesTree (El-Kebir, et al., 2015), EXPANDS (Andor, et al., 2014), and SCHISM (Niknafs, et al., 2015) revealed variable success rates, with some methods showing consistently poor accuracy. EXPANDS, which was designed for phylogeny reconstruction using one WES at a time, and ABSOLUTE, which is best known and most effective for estimating tumor purity, had consistently poor accuracy in our simulations. While SCHISM and AncesTree, which do not explicitly account for the full range of observed CNVs in tumors, were less accurate on simulations with CNVs. We concluded that explicit accounting for CNVs is required in order to approximate mutation frequencies accurately.

To address this challenge and improve mutation-frequency estimation from WES of tumors with genomic instability, we developed Chimæra: clonality inference from mutations across biopsies. Chimæra relies on multiple biopsies for the same tumor to, first, approximate CNVs and mutation frequencies; then, identify mutations with similar approximate frequencies and associate them with subclones; and, finally, to estimate the true frequencies of these mutations and the associated subclones. As is the case for estimates made by SCHISM, ABSOLUTE and other methods, Chimæra is not able to produce frequency estimates for all mutations. Frequencies are not estimated for mutations that could not be associated with subclones, and these estimates remain an open problem. Finally, to demonstrate that Chimæra is able to reconstruct subclones from tumor profiles we produced Chimæra-inferred subclones and resulting phylogeny from profiles of ten biopsies taken from a castration-resistant prostate cancer (CRPC) tumor.

Methods

We begin by formulating the phylogeny reconstruction problem in set-theoretic terms, which leads to a natural model for the effects of CNVs on mutated-read fractions in WES. We describe our methodology for simulating WES tumor profiles, as well as our efforts to deconvolve mutation frequencies from simulated data using ABSOLUTE, AncesTree, EXPANDS, SCHISM, and Chimæra. Finally, to demonstrate that Chimæra can be effectively applied to clinical data, we describe a reconstructed phylogeny from WES profiles of ten same-tumor CRPC biopsies.

Phylogeny reconstruction problem

Let $\Pi = \{a, b, c, \dots, n\}$ denote the set of mutations identified across a set of profiled biopsies S . The mutation burden in any given cell is given as a subset of Π , $\beta \subseteq \Pi$, or as an element of the power set over Π , $\mathcal{P}(\Pi)$ or \mathcal{P} for short; i.e. $\beta \in \mathcal{P}$ is a specific mutation ensemble that characterizes a tumor subclone. We denote the cellularity of β and its corresponding subclone in biopsy $s \in S$ as P_β^s , and the frequency of mutation $a \in \beta$ in biopsy s as $P_a^s = \sum_{\{\beta | \beta \in \mathcal{P}, a \in \beta\}} P_\beta^s$. Consequently, $\sum_{\beta \in \mathcal{P}} P_\beta^s = 1$ and the assignment $A = \{P_\beta^s | \beta \in \mathcal{P}, s \in S\}$ produces a solution to our clonality reconstruction formulation.

Mutation frequencies

As defined above, for a mutation a in biopsy $s \in S$, P_a^s denotes the frequency of cells in s with mutation a . The total copy number C_s of the allele targeted by the mutation can be estimated from WES data. C_s is composed of the copy numbers of the allele in cells that lack a , δ_s ; the copy number of the wildtype allele in mutated cells, δ_s^0 ; and the copy number of the mutated

allele, δ_s^a (Figure 3). Adopting the infinite-sites assumption, we denote the mutated-read fraction—the fraction of reads reflecting the mutated vs. wildtype allele in a WES profile—in sample s as f_s . Then, we can form the following equations (Eq. 1 and Eq. 2).

$$C_s = 2\delta_s(1 - P_a^s) + P_a^s(\delta_s^0 + \delta_s^a) \quad \text{Eq. 1}$$

$$f_s = \frac{P_a^s \delta_s^a}{C_s} \quad \text{Eq. 2}$$

Chimæra

Chimæra proceeds in three steps. First, mutation frequencies are estimated from sequencing and CNV data in each biopsy; then, mutations with similar frequency vectors (across biopsies) are clustered together to form subclones; and finally, mutation frequencies and CNVs for these alleles are refined using an optimization process. The optimization assumes that all clustered mutations that are associated with the same subclone have the same frequency in each tumor biopsy and that δ_s^a —the average copy number of the mutated allele—is the same across all biopsies from the same tumor.

A first approximation. We first approximate δ_s^a by accounting for tumor purity, i.e., the fraction of tumor cells in the biopsy, and assuming that the allele’s average copy number in tumor cells—whether mutated or not—is fixed. Let φ be the purity of the biopsy, then Eq.2 can be rewritten as follows:

$$f_s = \frac{P_a^s \delta_s^a \varphi}{C_s \varphi + 2(1-\varphi)} \quad \text{Eq. 3,}$$

C_s , in turn, can be approximated from the observed copy number C_{obs} as given in Eq. 4; C_{obs} can be estimated using additional biochemical assays, genomic sequencing, or through computational analysis of WES data (Koboldt, et al., 2012).

$$C_s = \frac{C_{obs} - 2(1-\varphi)}{\varphi} \quad \text{Eq. 4}$$

The simplifying assumption that the allele’s average copy number in tumor cells in each biopsy is equivalent produces a first approximation for its mutation frequency (Eq. 5). This constraint is later removed in the optimization process that follows.

$$\widetilde{P}_a^s = \frac{2f_s C_{obs}}{C_{obs} - 2(1-\varphi)} \quad \text{Eq. 5.}$$

Subclone reconstruction. Approximate mutation frequency vectors (Eq. 5) are then clustered using tclust (Fritz, et al., 2012) with the number of clusters selected by optimizing intra-cluster entropy or the sum of square errors (SSE), and using a variety of optimization methods including the Elbow method, Gaussian mixture decomposition (GMD), and SD index (Celeux and Govaert, 1995; Kovács, et al., 2005; Krzanowski and Lai, 1988). We evaluated each clustering methods on simulated data; e.g., in our simulations, SSE with the Elbow optimization method produced the best results for Chimæra frequency estimates, while SD index was the best for SCHISM. Each mutation cluster formed a subclone representation and was used to infer subclone frequencies and copy number estimates for each mutated allele.

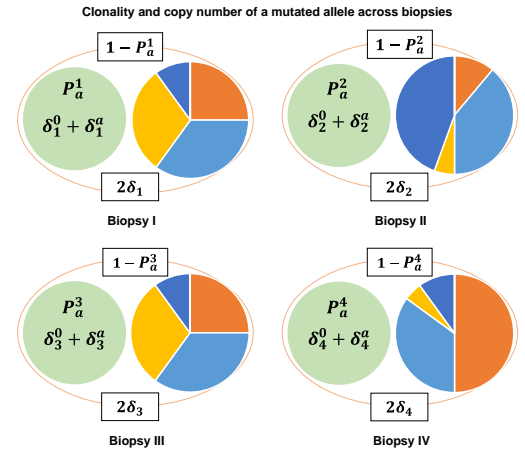


Figure 3. Our mutation-centric model for the effects of CNVs on mutated-read fractions in WES. In each biopsy s , the mutated-read fraction is a function of the true mutation frequency P_a^s and (1) the copy numbers of the allele in all profiled cells—tumor and WT—that lack this mutation, δ_s , and (2) the copy numbers of the wildtype and the mutated allele in tumor cells with the mutation, δ_s^0, δ_s^a .

Frequency and copy number inference. Focusing on subclone $\beta \in \mathcal{P}$, EQ. 3 describes a relationship between the frequencies and copy numbers of mutations in β , as given by Eq. 6. Here, $\mathcal{B}_{sa} \in \mathbb{R}^{|\mathcal{S}|, |\beta|}$ is fully determined from observations from sequencing assays, including the estimated copy numbers and observed mutated-read fractions for each subclone mutation.

$$P_a^s \delta_s^a = f_s \left(C_s + \frac{2}{\phi} - 2 \right) \equiv \mathcal{B}_{sa}, \quad \forall a \in \beta, s \in S. \quad \text{Eq. 6}$$

Eq. 6 mutation frequencies and copy numbers cannot be analytically decoupled, but same-subclone mutations are expected to have the same frequencies, i.e. $P_a^s = P_b^s \forall a, b \in \beta$. To simplify the optimization problem, we assume that copy numbers of each mutation are the same in each same-tumor biopsy, i.e. $\delta_{s_i}^a = \delta_{s_j}^a \in [0, CN] \forall s_i, s_j \in S$, where CN is a fixed upper bound for the copy number; $CN = 15$ in our simulations and WES analysis. While we expect that this assumption will introduce some errors to the approximation of δ_s^a , it will have limited effects on the selection of optimal mutation frequencies because the variability of copy number averages for the mutated allele across biopsy is expected to be low. We note that while this assumption may be appropriate for tumor profiles, it is violated by our simulations, which produced variable copy numbers for the same mutated allele across biopsies. Consequently, we pose an optimization problem based on Eq. 6, producing the following outer product of vectors \vec{P} and $\vec{\delta}$:

$$\min \|\vec{P} \otimes \vec{\delta} - \mathcal{B}\|_2, \quad \forall a \in \beta, s \in S; 0 \leq \delta^a \leq CN, 0 \leq P_s \leq 1, \quad \forall a \in \beta, \forall s \in S. \quad \text{Eq. 7}$$

Where \vec{P} is the mutation frequency vector across biopsies for all mutations in β ($|\vec{P}|=|\mathcal{S}|$); $\vec{\delta}$ is the copy-number vector for all mutations in β ($|\vec{\delta}|=|\beta|$); and \mathcal{B} is as given in Eq. 6. We used limited-memory Broyden–Fletcher–Goldfarb–Shanno optimization (Sheppard, et al., 2008) to find locally optimal solutions to the optimization posed in Eq. 7.

Simulation of WES data

WES simulations were based on phylogenies and associated cellularity matrices that describe ancestral relations between 6 to 12 subclones. These were either generated by us (see Figures 4A,B, Table S1 for representative phylogenies) or adapted from CITUP. Each subclone was associated with 20 to

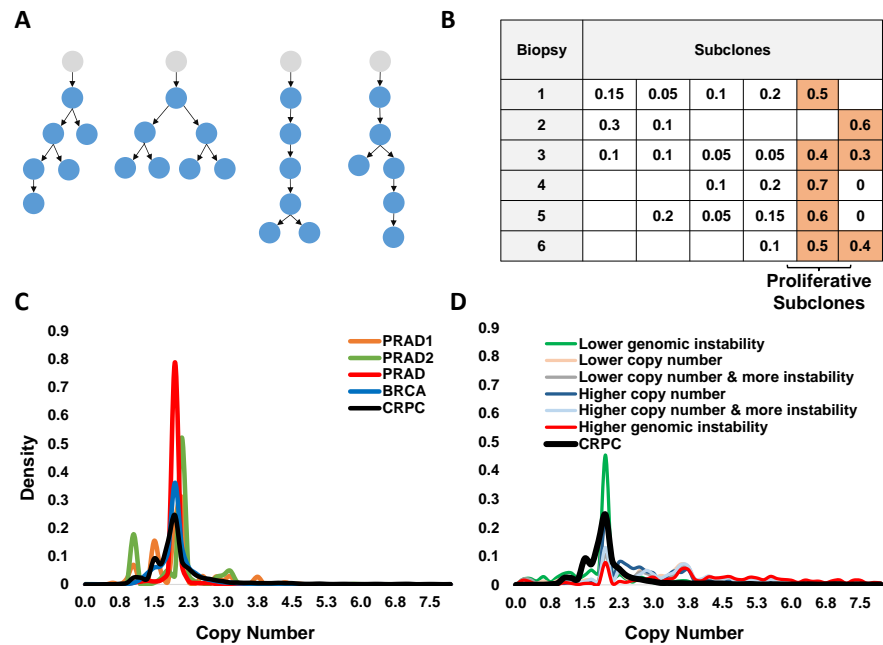


Figure 4. Our synthetic data generation and a comparison of simulated CNV distributions to those that were observed in tumors. (A) Representative phylogenies and (B) a representative cellularity matrix; see Table S1 (C) Density plots of average copy numbers across profiles of TCGA prostate (PRAD) and breast (BRCA) tumors, and our CRPC tumor. PRAD1 and PRAD2 show genome-wide CNV distributions in each of two PRAD tumors, while PRAD and BRCA distributions are taken across genes and tumors; CNVs ranged from 0 to >260x. (D) Simulated CNVs ranged from 0 to 15x.

50 somatic mutations, and each somatic mutation was associated with a trio of copy numbers— δ_s , δ_s^0 , and δ_s^a —that were taken from truncated normal distributions with means $\mu \in \{1,2,3\}$, where $\mu = 1$ corresponds to no copy number changes, and standard deviation $\sigma \in \{0,1,2,3\}$; $\sigma = 0$ was used only when $\mu = 1$. The resulting copy numbers model a range of genomic instability conditions that was in line with observed copy number changes in PRAD and BRCA tumors (Figure 4C,D). We assumed no linkage between simulated CNVs of any mutations. In addition, we added up to 10% of wildtype reads for all simulated mutations to account for the potential inclusion of non-tumor cells in the assay (WT subclone in Figure 1A). Total coverage for each allele—i.e. the number of reads covering both wild-type mutated genomic position—was taken by sampling mutation coverage values from our CRPC tumor biopsies. Finally, once idealized counts were available for both mutated and wild-type alleles, noise was added to simulate duplication or loss of up to 5% of the observations according to a uniform distribution. Each simulation was repeated to produce six biopsies per tumor using a distinct cellularity vector for each biopsy (as depicted in Figure 4A,B). The availability of six biopsies per tumor increases the likelihood that mutations can be aggregated and subclone mutation frequencies can be compared to infer ancestral relations. We note that while our CRPC tumor was profiled at ten regions, setting a six-biopsy minimum will exclude the profiling of many tumor types using our methods; this was a compromise between clinical feasibility and power to infer mutation frequencies and phylogenies.

Profiling and analysis of 10 CRPC biopsies

To test our ability to infer mutation frequencies and ancestral relations between subclones based on clinical profiles, we profiled 10 castrate-resistant prostate cancer (CRPC) tumor biopsies (Figure 5). The Specimen was collected at the Department of Pathology and Molecular Pathology, University Hospital Zurich, Switzerland as previously described (Mortezavi, et al., 2011) with the approval of Cantonal scientific ethics committee Zurich, approval number KEK-ZH-No. 2014-0007, and with informed consent by the patient. Tumor regions were selected for heterogeneous histological presentation by an experienced uropathologist (PJW). DNA from peripheral blood and FFPE punches (10 cylinders with diameter of 0.6 mm) was isolated with the Maxwell 16 LEV

Blood DNA kit (Promega, AS1290) and Maxwell 16 FFPE Tissue LEV DNA Purification Kit (Promega AS1130), respectively, according to manufacturer's recommendations; 300 μ l of blood collected in a BD Vacutainer K2 (EDTA 18.0mg) tube was added to 30 μ l of Proteinase K solution (final concentration 2 mg/ml) and subsequently mixed with 300 μ l lysis buffer, vortexed and incubated for 20 min at 56°C. FFPE

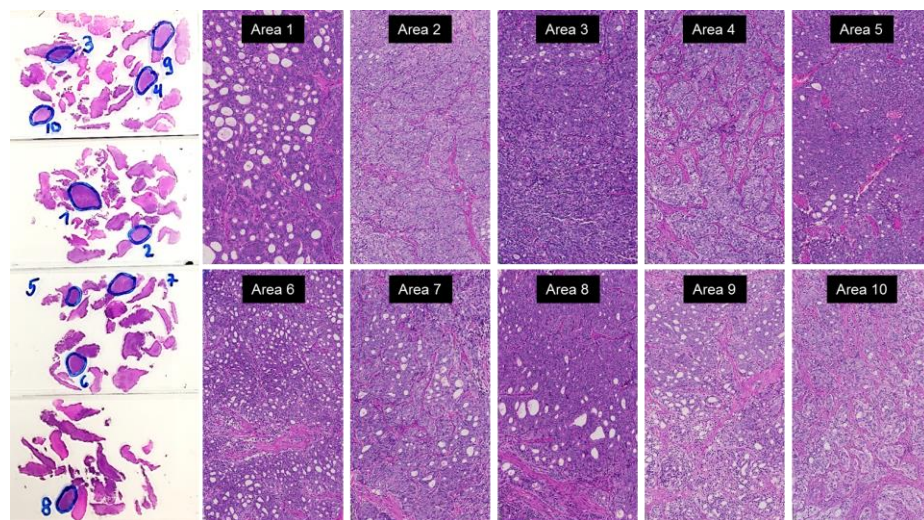


Figure 5. Profiled CRPC regions. Overview of four hematoxylin-eosin stained histology slides with 10 profiled areas (left); and zoomed-in versions (right) that portray the histological heterogeneity of this tumor. These CRPC regions were profiled by deep WES.

cylinders were deparaffinised with xylene, washed twice with ethanol, dried 10 min at 37°C and re-suspended in 200µl incubation buffer containing 2mg/ml Proteinase K. Samples were incubated overnight at 70°C and mixed with 400µl lysis buffer. Lysates from both, blood and FFPE tissues, were transferred to well 1 of the supplied cartridge of the corresponding kit and DNA was automatically purified and eluted in 30µl Tris-buffer, pH 8.0 by the Maxwell instrument. Each biopsy was profiled using Agilent SureSelect Whole Exome Enrichment, v6 (58 Mbp) and 2 × 75bp paired-end reads were used for optimal performance on a HiSeq 4000 (Illumina). Mutation calling was followed by protocols established by TCGA and ExAC (Lek, et al., 2016; The Cancer Genome Atlas, 2015). Reads were aligned to hg19 using BWA (Li and Durbin, 2010), and variants were called with GenomeAnalysisTK, MuTect (Cibulskis, et al., 2013), Picard MarkDuplicates, and additional post-processing utilities from GATK including BaseRecalibrator. FastQ files were deposited in EBI's ENA project PRJEB19193. Predicted mutations are given in Table S2; mutations were annotated with estimated read fractions and estimated CNVs by VarScan using default parameters and after setting the maximum amplification to 15x (Koboldt, et al., 2012). Mutations that were present in fewer than 3 biopsies or supported by fewer than 3 reads were discarded. A total of 355 mutations were used as input for inference methods.

Results

We describe our efforts to evaluate method accuracy on simulated data and to reconstruct phylogeny based on WES profiles of 10 CRPC biopsies.

Accuracy of mutation-frequency estimation based on simulated data

We compared the accuracy of EXPANDS, ABSOLUTE, SCHISM, AncesTree, and Chimæra on simulated data, as described in Methods. Phylogeny reconstruction success and clonality-inference accuracy by EXPANDS and ABSOLUTE were the lowest. EXPANDS relies on single biopsies, and when evaluated on phylogenies that were composed of as few as 3 tumor subclones, EXPANDS-reconstructed phylogenies from profiles of same-tumor biopsies (both simulated and collected from the clinic including the CRPC reported on here) had few common ancestral inferences and performance was poor in every tested simulated instance. In contrast, SCHISM-reconstructed phylogenies from synthetic constructions with 3 tumor subclones were accurate in 100% of tested instances. ABSOLUTE can process profiles of multiple biopsies per tumor and has good accuracy for inferring tumor purity in our synthetic data. However, when using default parameters, errors in ABSOLUTE frequency-inferences were more than double those of SCHISM. Parameter optimization through human intervention consistently improved its accuracy, but it remained less accurate than SCHISM. Moreover, the degree of human intervention that this required was not compatible with large-scale benchmarking. Consequently, we focused on accuracy comparisons between inferences by SCHISM, AncesTree, and Chimæra (as given in Figure 6), and excluded EXPANDS and ABSOLUTE from further analyses.

AncesTree accepts no external input when estimating mutation frequencies, but SCHISM and Chimæra can be guided by externally-inferred mutation clusters. SCHISM's implementation includes its own selected clustering methods, and these were also used to compare accuracy. We clustered mutations with tclust based on five optimization methods: ElbowSSE, Entropy, GMD, Mclust, and SDIndex. We compared the accuracy of methods and pipelines on 2000 simulated assays, including both simulated assays with and without modelled genomic instability (varying mutation copy numbers). The accuracy of SCHISM estimates was better on average than that of AncesTree, but it was relatively sensitive to clustering optimization methods, with SDIndex outperforming other methods, including those included in SCHISM's implementation. Comparatively, Chimæra estimates were less dependent on clustering methods and significantly outperformed estimates by SCHISM with SDIndex ($p < 1E-16$ by U test); Chimæra performance

was marginally best using ElbowSSE clustering (Figure 6A). A comparison of SCHISM and Chimæra on CITUP-simulated data (no CNVs) suggested similar accuracy for SCHISM-SDIndex and Chimæra-ElbowSSE ($p < 0.06$, based on 700 sim assays; Figure 6B).

Inference accuracy, for both SCHISM and Chimæra, was anti-correlated with the level of genomic instability, which followed truncated normal distributions with varying means and variances (Figure 6C, see Methods for data generation). To better understand mutation-level behaviour, as opposed to the genome-level comparisons in Figure 6C, we rescued individual mutations from each simulation and compared accuracy, mutation by mutation, as a function of their simulated copy numbers (Figure 6D). The result suggests similar Chimæra accuracy across copy numbers. We note that many mutations were eliminated from the evaluation by both the SCHISM and Chimæra pipelines. In total, only 40% and 20% of mutations were assigned frequencies by Chimæra and SCHISM, respectively; these proportion were independent of mutation copy numbers. While Chimæra assigned frequencies to all clustered mutations, SCHISM did not successfully estimate mutation frequencies for some simulated genomes. Accuracy comparisons in Figure 6 were made using only those mutations that had assigned frequencies by all methods.

In its totality, our analysis suggests that, at least under our model, mutation frequency estimation is more challenging for genomes with high copy-number variability. Chimæra inference accuracy for simulated genomes where all mutations had consistently low or consistently high copy numbers was relatively high. This is in part due to Chimæra's iterative process, where success in mutation clustering is followed by an optimization process that can correct for consistently high or consistently low mutation copy numbers.

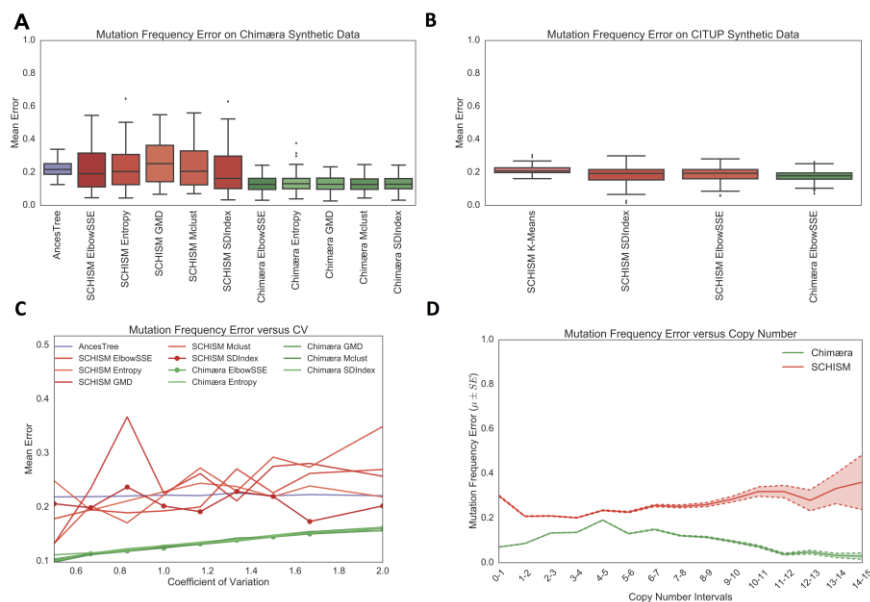


Figure 6. Accuracy on simulated data. (A) Accuracy of mutation-frequency estimates by AncesTree (purple), SCHISM (red) and Chimæra (green) on simulated WES data from genomes with varying mutation copy numbers; SCHISM and Chimæra were evaluated using multiple clustering methods with SDIndex (SCHISM) and ElbowSSE (Chimæra) producing top accuracy, respectively. (B) The gap between SCHISM and Chimæra accuracy was narrower on simulated data with no copy number variations. (C) Accuracy was inversely correlated with genomic instability, which was measured here as the coefficient of variation of the distributions used to simulate CNVs in each simulated WES profile; SCHISM with SDIndex clustering outperformed AncesTree inferences. (D) Evaluated independently, mutation copy numbers had relatively little effect on Chimæra accuracy. We report results for Chimera with ElbowSSE and SCHISM with SDIndex, but these are representative and resemble results with other clustering methods. Standard errors are reported. Mean Error is the mean of L1 distances between true and estimated mutation frequencies after normalizing for the number of biopsies.

Phylogeny inference in CRPC

To test our ability to infer mutation frequencies and ancestral relations between subclones using clinical data, we profiled ten biopsies of a single castrate-resistant prostate cancer (CRPC) tumor (Figure 5). CRPCs are high-risk prostate tumors that are known to have high genomic instability (Robinson, et al., 2015). Each of these biopsies was profiled and analyzed as described in Methods, producing a total of 355 mutations that were used as input to SCHISM, ABSOLUTE and Chimæra (Table S2). SCHISM did not produce frequency estimates for any of the mutations in Table S2.

ABSOLUTE, following repeated parameter optimization steps by PC (author), produced frequency estimates for 21 mutations, resulting in 4 predicted subclones; mutations in 3 of these subclones had high frequencies in at least one biopsy, but ancestral relations between these subclones could not be inferred. Chimæra inferred frequencies for 31 mutations that were clustered into 8 subclones, and these formed a unique phylogeny and resulting cellularity estimates. A summary of Chimæra inferences is given in Figure 7 with subclones, and both mutation frequencies and cellularities are given in Table S2.

Chimæra inferred potentially initiating mutations that targeted 7 genes, and identified a chain of 3 subclones that followed in a later stage in tumor evolution; the earliest 2 subclones were nearly eliminated from the tumor, suggesting that the following 2 subclones had a selective advantage. The inference suggests a diverging event associated with subclone 5 and 7 mutations, which resulted in the proliferation of new subclones. Interestingly, the analysis identified genes that were targeted by multiple mutations, with these mutations inferred from multiple subclones and specific evolutionary sequence of this tumor (ZNF778 and ANKRD36B; see Figure 7).

Discussion

We sought to develop a methodology to improve the accuracy of tumor phylogeny reconstruction from tumor WES data by improving mutation-frequency estimates when multiple profiles of the same tumor are available. Mutation-frequency estimates are particularly challenging in the face of high genomic instability, which is characteristic to many tumor types, including the high-risk prostate cancer tumor whose profiling was reported on here. Our proposed method, Chimæra, is suitable for analyzing tumor profiles across multiple time points and across multiple tumor regions and can be easily modified to process both types of data, but here we focused the discussion on the latter. In addition, while we focused on single nucleotide variants, our methods can be extended to consider other types of genomic alterations.

We outlined the challenges involved in estimating mutation frequencies from WES of genomes with high genomic instability—where the copy numbers of mutations can widely vary. We showed that, even for EXPANDS, which uses the copy number of mutations to infer phylogeny,

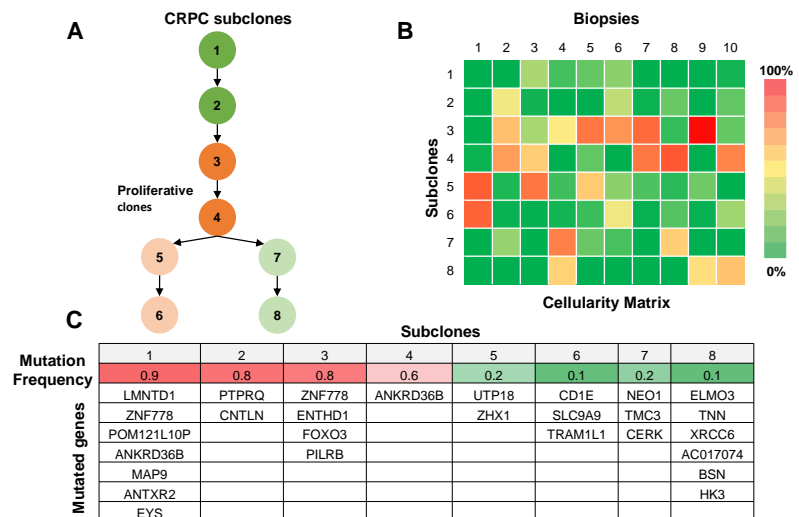


Figure 7. Reconstructed tumor phylogeny. (A) Chimæra inferred 8 CRPC subclones that implied a recently diverging phylogeny, with subclones 3-5 the most proliferative according to the resulting (B) cellularity matrix. (C) Mutated genes and mutation average frequencies across biopsies in each subclone.

the accuracy of mutation frequency estimates, cellularities, and phylogeny reconstruction using single biopsies was very poor. Our own investigation suggests that the task is often impossible on simulated assays with varying mutation copy numbers. Consequently, we elected to rely on multiple biopsies per tumor to improve mutation-frequency estimation. We showed that even when profiles of multiple biopsies are available, methods that do not explicitly account for the full range of copy number variability produce inconsistent results with often poor accuracy.

Chimæra is able to improve mutation-frequency estimates by harnessing added information from multiple profiles and by directly accounting for the influence of CNVs on observations from WES. Chimæra's advantage was clearly observed in simulated data, where its performance was the most consistent, and its accuracy the greatest. Interestingly, while Chimæra was able to estimate mutations frequencies with relatively high accuracies even for mutations with very high and very low copy numbers, its performance declined for the most unstable genomes where mutation copy numbers varied widely. Our CRPC tumor, which displays high genomic instability, exemplified this problem. Chimæra estimated frequencies for only 40% of mutations in simulated data and only 10% of mutations in our CRPC-biopsy profiles. This difference is likely to be due to the number of mutations associated with the formation of each subclone and suggests that future work should further vary this number.

In conclusion, our results suggest that accurate mutation-frequency and cellularity inference is possible using profiles of multiple biopsies per tumor. Improving current estimates further—both in terms of accuracy and by including more mutations in estimates—remains an open challenge.

Acknowledgements

This project was funded by the European Union's Horizon 2020 research and innovation programme under grant agreement 668858 to PJW, MRM, and PS; and in part by the Foundation for Research in Science and the Humanities at the University of Zurich to PJW, and by Texas Children's Cancer Center and Cookies for Kids' Cancer Foundation to PS.

Supplementary Materials

Tables S1 and S2, which include phylogenies and cellularity matrices used in simulations, and mutations and inferences from CRPC profiles are available from GitHub, project Chimaera.

Bibliography

- Andor, N., *et al.* Pan-cancer analysis of the extent and consequences of intratumor heterogeneity. *Nature medicine* 2016;22(1):105-113.
- Andor, N., *et al.* EXPANDS: expanding ploidy and allele frequency on nested subpopulations. *Bioinformatics* 2014;30(1):50-60.
- Boutros, P.C., *et al.* Spatial genomic heterogeneity within localized, multifocal prostate cancer. *Nature genetics* 2015;47(7):736-745.
- Carter, S.L., *et al.* Absolute quantification of somatic DNA alterations in human cancer. *Nature biotechnology* 2012;30(5):413-421.
- Celeux, G. and Govaert, G. Gaussian parsimonious clustering models. *Pattern recognition* 1995;28(5):781-793.
- Cibulskis, K., *et al.* Sensitive detection of somatic point mutations in impure and heterogeneous cancer samples. *Nature biotechnology* 2013;31(3):213-219.
- Cieslik, M., *et al.* The use of exome capture RNA-seq for highly degraded RNA with application to clinical cancer sequencing. *Genome research* 2015;25(9):1372-1381.
- El-Kebir, M., *et al.* Reconstruction of clonal trees and tumor composition from multi-sample sequencing data. *Bioinformatics* 2015;31(12):i62-i70.
- Fidler, I.J. and Hart, I.R. Biological diversity in metastatic neoplasms: origins and implications. *Science* 1982;217(4564):998-1003.

Fritz, H., Garcia-Escudero, L.A. and Mayo-Iscar, A. tclust: An R package for a trimming approach to cluster analysis. *Journal of Statistical Software* 2012;47(12):1-26.

Futreal, P.A., et al. A census of human cancer genes. *Nat Rev Cancer* 2004;4(3):177-183.

Gao, R., et al. Punctuated copy number evolution and clonal stasis in triple-negative breast cancer. *Nature Genetics* 2016.

Getz, G. and Ardlie, K. Mutation Analysis in Frozen and FFPE Tumor Samples. In: Meyerson, M. and Shmulevich, I., editors, *TCGA Second Annual Scientific Symposium*. Crystal City, Virginia: National Institutes of Health; 2012.

Gundem, G., et al. The evolutionary history of lethal metastatic prostate cancer. *Nature* 2015;520(7547):353-357.

Higgins, M.E., et al. CancerGenes: a gene selection resource for cancer genome projects. *Nucleic acids research* 2007;35(Database issue):D721-726.

Jiao, W., et al. Inferring clonal evolution of tumors from single nucleotide somatic mutations. *BMC bioinformatics* 2014;15:35.

Koboldt, D.C., et al. VarScan 2: somatic mutation and copy number alteration discovery in cancer by exome sequencing. *Genome research* 2012;22(3):568-576.

Kovács, F., Legány, C. and Babos, A. Cluster validity measurement techniques. In, *6th International symposium of hungarian researchers on computational intelligence*. Citeseer; 2005.

Krzanowski, W.J. and Lai, Y. A criterion for determining the number of groups in a data set using sum-of-squares clustering. *Biometrics* 1988:23-34.

Lek, M., et al. Analysis of protein-coding genetic variation in 60,706 humans. *Nature* 2016;536(7616):285-291.

Li, H. and Durbin, R. Fast and accurate long-read alignment with Burrows–Wheeler transform. *Bioinformatics* 2010;26(5):589-595.

Malikic, S., et al. Clonality inference in multiple tumor samples using phylogeny. *Bioinformatics* 2015;31(9):1349-1356.

Mann, K.M., et al. Analyzing tumor heterogeneity and driver genes in single myeloid leukemia cells with SBCapSeq. *Nature biotechnology* 2016.

Mortezavi, A., et al. KPNA2 expression is an independent adverse predictor of biochemical recurrence after radical prostatectomy. *Clinical cancer research* 2011;17(5):1111-1121.

Niknafs, N., et al. SubClonal Hierarchy Inference from Somatic Mutations: automatic reconstruction of cancer evolutionary trees from multi-region next generation sequencing. *PLoS computational biology* 2015;11(10):e1004416.

Nowell, P.C. The clonal evolution of tumor cell populations. *Science* 1976;194(4260):23-28.

Robinson, D., et al. Integrative clinical genomics of advanced prostate cancer. *Cell* 2015;161(5):1215-1228.

Sheppard, D., Terrell, R. and Henkelman, G. Optimization methods for finding minimum energy paths. *The Journal of chemical physics* 2008;128(13):134106.

Suzuki, H., et al. Mutational landscape and clonal architecture in grade II and III gliomas. *Nature genetics* 2015;47(5):458-468.

The Cancer Genome Atlas. Comprehensive molecular portraits of human breast tumours. *Nature* 2012;490(7418):61-70.

The Cancer Genome Atlas. The molecular taxonomy of primary prostate cancer. *Cell* 2015;163(4):1011-1025.

Wang, J., et al. Tumor evolutionary directed graphs and the history of chronic lymphocytic leukemia. *eLife* 2014;3.

Wang, Y., et al. Clonal evolution in breast cancer revealed by single nucleus genome sequencing. *Nature* 2014;512(7513):155-160.